Sustainable and Resilient Infrastructure

ISSN: (Print) (Online) Journal homepage: www.tandfonline.com/journals/tsri20

Analytical fragility curves for trees subject to ice loading in a changing climate

R. Campos, P. S. Harvey Jr & G. Hou

To cite this article: R. Campos, P. S. Harvey Jr & G. Hou (2023) Analytical fragility curves for trees subject to ice loading in a changing climate, Sustainable and Resilient Infrastructure, 8:6, 555-571, DOI: 10.1080/23789689.2023.2202962

To link to this article: https://doi.org/10.1080/23789689.2023.2202962

Published online: 09 May 2023.

SUSTAINABLE AND RESILIENT INFRASTRUCTURE
2023, VOL. 8, NO. 6, 555–571
https://doi.org/10.1080/23789689.2023.2202962

Analytical fragility curves for trees subject to ice loading in a changing climate

R. Campos, P. S. Harvey Jr and G. Hou

School of Civil Engineering and Environmental Science, University of Oklahoma, Norman, OK, USA

ABSTRACT

Recent severe ice storms across the United States severely damaged trees resulting in extensive electrical power outages. Furthermore, trees and branches can fall on nearby roads, blocking traffic flow and reducing the safety of drivers. In this study, trees subjected to ice loads were analyzed using the finite element method and Monte Carlo simulation to develop analytical fragility curves. Two-dimensional, fractal trees were constructed with randomly generated geometric and mechanical parameters for four deciduous tree species: *Acer saccharum*, *Tilia americana*, *Fagus grandifolia*, and *Quercus alba*. Two load case scenarios were considered – with and without the effects of leaves – which were then subjected to varying ice accumulation thicknesses. The resulting fragility curves suggest that leaves have a substantial impact on tree branch damage under ice loads, which is significant because of the increase in unseasonably early ice storms due to climate change.

ARTICLE HISTORY
Received 10 August 2022
Accepted 6 March 2023

KEYWORDS
Severe ice storm; analytical fragility; hazard; Monte Carlo sampling

1. Introduction

Recent severe ice storms across the United States, namely, in Oklahoma and Texas, severely deformed and damaged trees resulting in extensive electrical power outages (National Weather Service, 2020b, 2021). Reports from the National Weather Service (2020a,b) show ice accretions of up to 38.1 mm during the October 2020 Oklahoma ice storm – Oklahoma's earliest ice storm in the climatological record – which damaged trees and electrical components and caused multiple electrical outages. Furthermore, the destructive interactions between trees and electrical components during these ice storms have been observed to be significant (Call, 2010; Degelia, Christian, Basara, et al., 2016; Ismay, 2020). Ice storms are particularly hazardous to the electrical infrastructure because ice accretion on the electrical transmission and distribution system components (e.g., electrical poles and lines) can directly damage them, but also nearby trees laden with ice have the potential to (a) come in contact with lines causing electrical arcing or (b) bear or fall on electrical power lines failing the components (Call, 2010).

Further, repairing the electrical transmission and distribution systems after a severe ice storm can be costly, often costing millions or billions of dollars (Tropea & Stewart, 2021). For example, the October 2020 Oklahoma ice storm, which was declared a major disaster (4575-DR-OK) by the Federal Emergency Management Agency (FEMA, 2023), has been obligated over $100 M in total public assistance grants and over $4.5 M from FEMA Hazard Mitigation Grant Program (HMGP) as of 16 February 2023. The HMGP obligation is about three times that of 2022 Florida Hurricane Ian (DR-4673-FL), which received about six times as much in public grant assistance. In the past decade, FEMA has granted hundreds of millions of dollars and has declared 20 severe ice storms as major disasters in the United States, nine of which were declared major disasters since 2020 (FEMA, 2023). Because climate change has been increasing the frequency and intensity of severe weather (Mostafavi, 2018), including ice storms (Klima & Morgan, 2015; Kovacik & Kloesel, 2014), it is important to understand and mitigate the resulting failure of critical electrical infrastructure components (Aktan, Brownjohn, Moon, et al., 2022; Khan & Conway, 2020; Swaminathan, Sridharan, & Hayhoe, 2018).

During extreme events, such as ice storms and hurricanes, fallen trees can cause widespread disruption to critical infrastructure systems (CIS) such as power and transportation systems. For example, tree failures are responsible for about 55.2% of distribution system failures in the Northeast US (Li, Zhang, Luh, et al., 2014). It can take up to months to remove tree debris from roads following hurricanes (Laefer & Pradhan, 2006), not only hindering the emergency response immediately after extreme hazards but also affecting the recovery of other lifeline infrastructure in the recovery phase. Despite the severe consequences caused by fallen trees, very little effort has been put into modeling tree fragility

CONTACT P. S. Harvey Jr harvey@ou.edu;

and assessing tree-induced risk to CIS. Currently, a range of studies have attempted to model the tree fragility following extreme winds and hurricanes (Ciftci, Arwade, Kane, et al., 2014; Hou & Chen, 2020; Kakareko, Jung, & Ozguven, 2020). However, most of them used simplified structural models of trees, focusing primarily on trunk failures, without considering branches or leaves. These simplified models are unable to capture the branch deflection, branch and leaf weight distribution throughout the tree, or any resulting branch failure, which could lead to inaccurate failure probabilities. Moreover, these studies are limited to wind hazards; fragility models of trees subjected to ice storms are still missing. As a result, no literature was found that considers tree-induced risk in the resilience/performance assessment of CIS subjected to ice storms, although a few studies have considered the impact of wind-caused tree damage on the resilience of CIS (Hou & Chen, 2020; Ma, Chen, & Wang, 2018; Tari, Sepasian, & Kenari, 2021). Severe ice storms generally occur during the winter season between December and March (Dolce & Erdman, 2022; Semonin, 1987), such as the December 2000 and December 2007 Oklahoma ice storms (National Weather Service, 2000, 2007), but a recent ice storm in Oklahoma occurred in October 2020 (National Weather Service, 2020b), which had a significant impact due to trees still having their leaves (Ismay, 2020). Researchers have attempted to quantify ice damage to trees (Brommit,
Charbonneau, Contreras, et al., 2004; Takahashi, Arii, & Lechowicz, 2007), but none has compared the differences between trees subjected to ice loads with and without the effects of leaves. Further, no attempts have been made to analytically model trees subjected to ice loads with the effects of leaves. However, research has been conducted to analytically model trees subjected to wind loads, with and without the effects of leaves (Ciftci, Arwade, Kane, et al., 2014).

Trees are naturally complex, so it is beneficial to simplify the geometry when constructing tree models (Khiripet, Viruchpintu, Maneewattanapluk, et al., 2010; Picard, Saint-André, & Henry, 2012). Further, tree and plant structures are generally modeled with only the trunk and branches (Honda & Hatta, 2004; Honda, Tomlinson, & Fisher, 1981, 1982; Jinasena & Sonnadara, 2013; Khiripet, Viruchpintu, Maneewattanapluk, et al., 2010; Lindenmayer & Prusinkiewicz, 1996; Wang, Zhao, & Qi- Xing, 2001). A fractal, a reoccurring geometric shape, is used to simulate many naturally occurring patterns and is simple to generate with a computer (Harmon, 2012; Saupe, 1988). Fractal generation is a common method for modeling trees, branches, and plants and is accomplished by implementing algorithms based on, for example, the Cantor set or the Lindenmayer system (Harmon, 2012; Khiripet, Viruchpintu, Maneewattanapluk, et al., 2010; Lindenmayer & Prusinkiewicz, 1996; Napolitano, 2015). Symmetrically branching (binary) fractal trees are iterated function system fractals that are created by drawing an initial pattern, transforming that initial pattern, and then combining the transformed and initial patterns (Kak, 2022). Binary fractals are defined by a branch-trunk scale factor r and tree- branch angle ϑ (Gulick, 2011; Kak, 2022). Further, the trunk bifurcates at the top resulting in a branch on either side of the trunk with each branch having a length of r times the height of the trunk (Gulick, 2011). In a fractal, the tree branch's diameter decreases with each successive iteration and is dependent on tree species, branch length, branch weight, and environment (Wang, Zhao, & Qi- Xing, 2001). There are two main methods for determining the biomass of a tree: by directly measuring the weight in the field or by using allometric equations (Picard, Saint- André, & Henry, 2012). Allometric equations, regression equations based on a linear or nonlinear correlation between the increases in tree dimensions, are commonly used to estimate the biomass of a tree or multiple trees (Picard, Saint-André, & Henry, 2012). The biomass of a tree is usually divided into sections, such as the trunk, bark, branches, leaves, large and medium-size roots and small roots (Picard, Saint-André, & Henry, 2012). The geometric and mechanical properties of multiple tree species have been recorded (Forest Products Laboratory, 1999; Jenkins, Chojnacky, Heath, et al., 2004), and researchers have used them to develop and analyze tree models (Hou & Chen, 2020). Tree vulnerability due to the December 2007 Oklahoma ice storm has been assessed using remote sensing (RS) and geographic information systems (GIS) (Rahman, 2010). Consequently, the critical factors resulting in tree damage from the December 2007 Oklahoma ice storm, ordered from most severe to least severe, were determined to be ice thickness, tree branch angle, pre-storm tree crown, wind, stem and branch diameters (Rahman, 2010).

A fragility curve, commonly used in seismic risk analysis (Guidotti, Chmielewski, Unnikrishnan, et al., 2016; Sharma, Tabandeh, & Gardoni, 2018), is a conditional failure probability of an element for a given hazard intensity measurement (Ansari, Rao, & Jain, 2022; Pitilakis, Crowley, & Kaynia, 2014; Zentner, Gündel, & Bonfils, 2017). Further, in seismic risk

analysis, fragility curves play a crucial role in establishing a connection between the probabilistic seismic hazard analysis (PSHA) and the effects of the predicted ground motion on infrastructure components (Pitilakis, Crowley, & Kaynia, 2014).

Additionally, seismic fragility curves are continuous functions that describe the probability of exceeding a set of particular building or infrastructure component limit states for a specific ground motion intensity measurement (e.g., peak-ground acceleration or peak-ground displacement) (Erberik, 2014; Pitilakis, Crowley, & Kaynia, 2014). Hazus, a standardized risk modeling methodology developed by FEMA (2003), utilizes fragility curves to assess the risk of building, electrical and transportation infrastructure components. Hazus considers four or five discrete damage states – none, slight, moderate, extensive, or complete – where each damage state's definition is based on the structure type and hazard (Kircher, Nassar, Kustu, et al., 1997). Currently, Hazus utilizes fragility curves for various structures subjected to hazards, such as earthquakes, floods, tsunamis and hurricanes. An effort has been made to develop fragility curves for urban or deciduous trees subjected to wind loads (Ciftci, Arwade, Kane, et al., 2014; Hou & Chen, 2020), but no literature was found that developed or analyzed the fragility curves of analytical tree models subjected to ice loads. However, Proulx and Greene (2001) empirically studied the relationship between ice thickness and tree damage (crown loss) for hardwood trees without leaves, which is in a way similar to a fragility curve.

In order to fill this gap in the literature, fractal trees subjected to ice loads were analyzed using the finite element (FE) and Monte Carlo sampling methods to develop fragility curves. The generation of fractal trees, formulation and analysis of the FE model and the development of the fragility curves are described in Section 2. The resulting fragility curves and the development of a method for estimating the fallen weight of a failed tree branch are discussed in Section 3 followed by concluding remarks in Section 4.

2. Methods

Four common hardwood tree species—*Acer saccharum* (Sugar Maple), *Tilia americana* (American Beech), *Fagus grandifolia* (American Basswood), and *Quercus alba* (White Oak)—were studied. In order to model and analyze these deciduous trees, which are highly variable and geometrically complex, a few assumptions had to be made (Picard, Saint-André, & Henry, 2012). The tree was modeled as a two- dimensional fractal and only includes the trunk and branches (Figure 1(a)).

The smaller branches and leaves, which grow from the large branches, were not modeled geometrically and instead were added as loads on the larger branches by utilizing allometric equations obtained from the literature. MATLAB (MathWorks, 2021) was used to model two-dimensional trees subjected to ice loads and develop fragility curves by using the Monte Carlo sampling method with a total of 40,000 quasi-static simulations. Two load cases were considered: load case 1 includes the loads due to the weight of the branches and ice on the branches; and load case 2 includes the same loads as case 1 but with the addition of loads due to the weight of the leaves and ice on the leaves. A total of 10,000 randomly generated two-dimensional trees were utilized in two analyses (cases 1 and 2) per species. Fifty ice load cases, ranging from 0 to 50.8 mm of ice thickness were used in both load cases 1 and 2. Ice thickness was used as an intensity measurement (Proulx & Greene, 2001), and the range of ice thickness used in this study is based on historical observations and the ice thickness maps provided in the ASCE/SEI 7–16 Standard (ASCE, 2017). OpenSees (McKenna & Feneves, 2000) was used to construct and solve the two-dimensional FE model subjected to both load cases 1 and 2 and the resulting total stresses were then compared to the modulus of rupture (MOR), which measures the bending strength, of the tree species to determine if the tree had failed. The failure criteria were based on the total stresses exceeding the MOR in sections that were categorized by successive fractal iterations and branches.

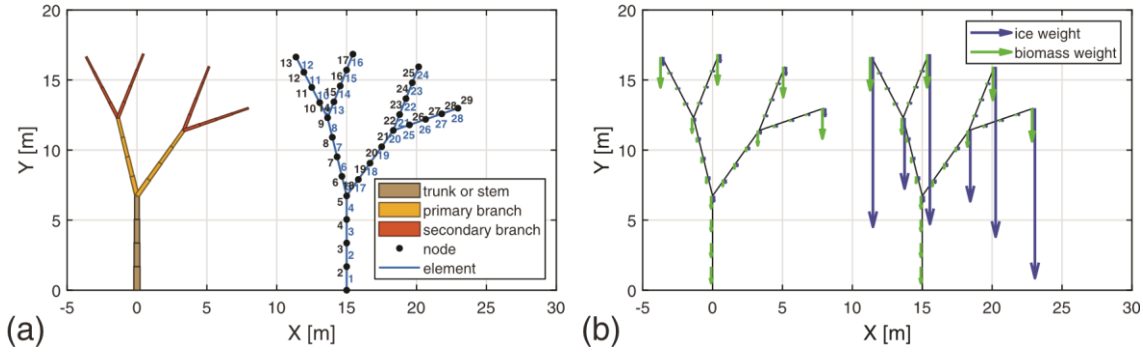

Figure 1. Visualization of model: (a) tree branch segments (left) and finite element model (right), and (b) weight comparison between load case 1 (left) and load case 2 (right) considering biomass and ice loads at t_{ice} ¼ 25:4 mm.

2.1. Two-dimensional fractal tree

A MATLAB script, FraktalT (Dmitry, 2021), was used to generate two-dimensional fractal trees, which requires specific input arguments: number of branch iterations, branch-trunk scale factor (r), tree-branch angle (ϑ), and trunk X- and Y-coordinates. The number of branch iterations refers to the number of branches that are generated beginning from the end (or top) of the tree's trunk. The branch-trunk scale factor (r) scales the branches relative to the length of the tree's trunk, and the tree-branch angle (ϑ) orientates the branches relative to the Y-axis. Three branch iterations were considered in the development of each tree's geometric dimensions and load estimations. Due to the computationally expensive nature of Monte Carlo simulation, only two branch iterations were considered for the FE analysis to keep the computational time and output data size to a reasonable amount, while still capturing the branching nature of the tree.

A fractal tree was randomly generated and then discretized into 28 elements with the trunk, the first fractal iteration, and the second fractal iteration being composed of 4, 8, and 16 elements, respectively. Figure 1(a) shows the FE discretization of a representative fractal tree. The geometric properties for each element were calculated based on the length of each element and the tree diameter at breast height (DBH) where the DBH is measured 1.37 m from the ground. The height (H) of the tree was estimated by using an exponential regression equation (Kenefic & Nyland, 1999) that is based on the DBH of the hardwood sugar maple tree and is given by

$$H = 1.3 + 36.86\exp[-15.4/(100 \times \mathrm{DBH} + 3.8)] \quad (\text{in meters}) \tag{1}$$

where DBH is in meters. Reliable species-specific allometric equations or parameters were not found in the literature; consequently, Equation 1 is used to calculate the height for each tree species in this study. The trunk's height (h_t) was then estimated relative to the height (H) of the tree as h_t¼ 0:24H, which is based on an estimate by McPherson and Peper (2012) for a 60-year-old hardwood green ash tree (*Fraxinus pennsylvanica*). The X- coordinate of the trunk was always taken as zero (i.e., perfectly straight, vertical trunk).

This model considers a linear decrease in branch diameter where each branch bifurcation (branching) results in equivalent areas between the two resulting branches (i.e., primary branches from the trunk and secondary branches from the primary branch), as shown in Figure 1(a). Further, to complement the linearity that is common in fractal tree iterations (Gulick, 2011; Kak, 2022; Lindenmayer & Prusinkiewicz, 1996), a linear scaling approach was employed to calculate the radius of each element by utilizing the ratio of the branch path length (l_p) to the total branch path length ($l_{p;\mathrm{total}}$). The total branch path length ($l_{p;\mathrm{total}}$) defines the total path length for a three iteration fractal and is given by

$$l_{p,\mathrm{total}} = h_t + h_t r + h_t r^2 + h_t r^3 \tag{2}$$

All paths in a fractal tree have the same total path length ($l_{p;\mathrm{total}}$). In Equation 2, a path is considered to begin at the base of the tree and finish at the end of a branch in the third iteration fractal. Because the development of the tree's FE model considers only two fractal iterations, there are only four possible total branch paths. The radius of an element is taken to be

$$r_e = \frac{\mathrm{DBH}}{2}\left(1 - \frac{l_{p,e} - l_{p,1}}{l_{p,\mathrm{total}}}\right) \tag{3}$$

where $l_{p;e}$ is the length along the branch path from the base of the tree to the center of the element, and $l_{p;1}$ is the path length to the center of the first element, which is equal to 0:5 h_t=4. Equation 3 ensures that the element at the base of the tree has a diameter equal to the DBH. The volume (V_e) for each element was calculated assuming a cylindrical element. The element's mass was then estimated based on V_e and the density (ρ) of the wood.

2.2. Generating random parameters

Monte Carlo sampling is used to propagate uncertainties in tree parameters – both geometric and material – to the fragility functions. The randomly generated geometric parameters used to develop the two-dimensional tree are DBH, r, and ϑ; the random material parameters are density of wood (ρ), modulus of elasticity (E), and MOR. No literature was found for the common distributions of these tree parameters. Further, there is a general confusion in the wood science research community as to which type of distribution is suitable for E and MOR (Owens, Verrill, Shmulsky, et al., 2019). Consequently, a uniform distribution is assumed:

$$U \overset{\text{i.i.d.}}{\sim} \mathcal{U}[a, b] \tag{4}$$

for random variable U 2 fDBH*; r; ϑ; ρ; E;* MORg where a and b are the minimum and maximum values,

Table 1. Lower (a) and upper (b) bounds used for uniform random variables for different tree species investigated herein.

		Tree Species			
Random variable	Bounds	Sugar Maple	Beech	Basswood	White Oak
DBH [m]	a	0.06	0.11	0.16	0.11
	b	0.70	0.62	0.68	0.66
r [–]	a	0.56	0.50	0.62	0.70
	b	0.96	0.92	0.91	0.93
ϑ [rad]	a	0.040	0.080	0.010	0.080
	b	0.660	0.750	0.480	0.870
ρ [kg/m^3]	a	560	560	320	600
	b	630	640	370	680
E [MPa]	a	10,700	9,500	7,200	8,600
	b	12,600	11,900	10,100	12,300
MOR [MPa]	a	65	59	34	57
	b	109	103	60	105

respectively. The typical ranges for the DBH, ρ, E and MOR of wood used in this study were determined by other researchers (Forest Products Laboratory, 1999; Jenkins, Chojnacky, Heath, et al., 2004). The bounds for ρ, E, and the MOR are based on the moisture content of the wood, where the lower bound is at a green cut or 100% moisture content and the upper bound is at 12% moisture content (Forest Products Laboratory, 1999). The bounds for r and ϑ for specific species of trees were not found in the literature and are therefore based on the observations of multiple tree species. Table 1 shows the a and b values for various tree species used in this study, and Figure 2 shows the variation of the fractal tree for each species due to the uniformly distributed variables with 100 realizations.

2.3. Load cases

The term ‘large branch’, or simply ‘branch’, is used to describe the mass of wood that sprouts from the trunk or stem. In this study, fractal iterations are comprised of branches, where each branch is

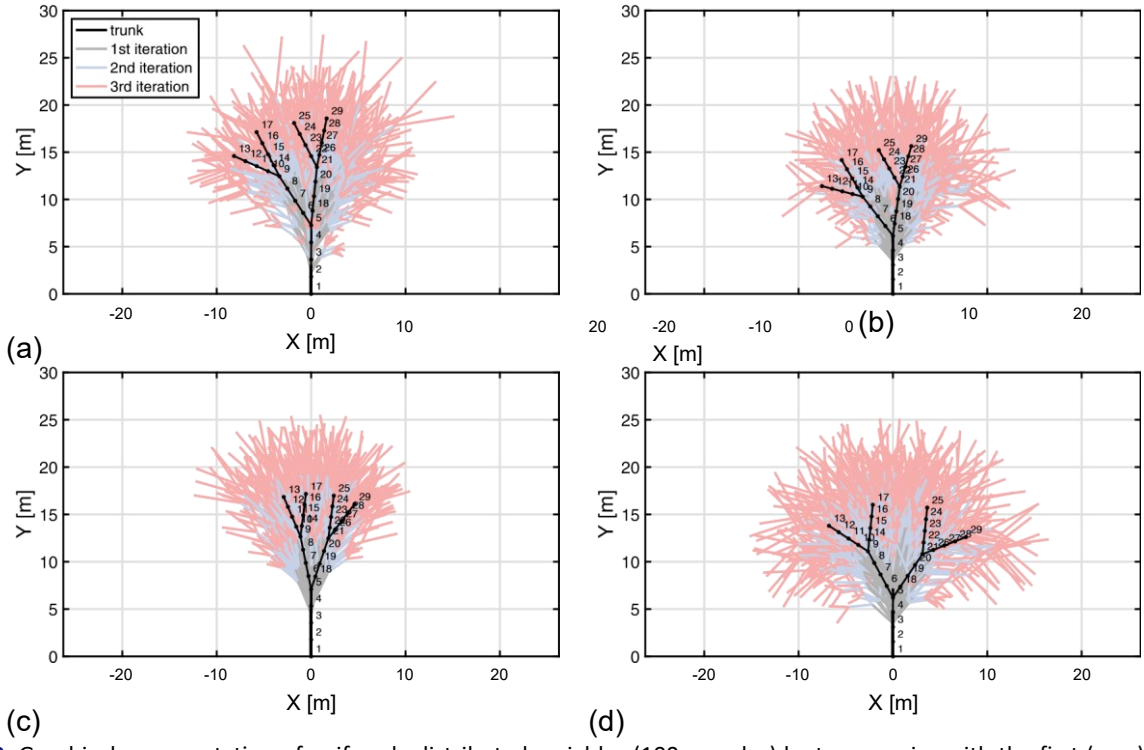

Figure 2. Graphical representation of uniformly distributed variables (100 samples) by tree species with the first (gray), second (blue), and third (red) iterations: (a) sugar maple, (b) beech, (c) basswood, and (d) white oak.

discretized into elements. The branch may split further into smaller branches, which are considered to bear the weight of the foliage or leaves. For load cases 1 and 2, an element's mass was calculated based on the volume of the cylinder and the density ρ of the wood, and the weight of each element was then calculated by multiplying this mass by gravitational acceleration g ¼ 9:81 m/s^2. The total biomass (MÞ of the tree, which includes the mass of the branches and leaves, was separated into foliage and small branch mass components, and M was calculated using a logarithmic regression equation from the literature of the form

$$M = \exp[\beta_0 + \beta_1 \ln(\mathrm{DBH})] \tag{5}$$

where β_0 and β_1 are regression parameters for hardwood species, such as Maple, Oak or Beech (Jenkins, Chojnacky, Heath, et al., 2003).

For load case 1, the small branch mass component (M_B) was utilized to approximate the mass of smaller branches that could not be captured by the branch mass calculations and is given by

$$M_B = M \exp\left[-1.6911 + \frac{0.8160}{100 \times \mathrm{DBH}}\right] \tag{6}$$

where DBH is in meters. Comparatively, for load case 2, the foliage mass component (M_F) was utilized in addition to the branch mass component where the foliage mass component is estimated by

$$M_F = M \exp\left[-4.0813 + \frac{5.8816}{100 \times \mathrm{DBH}}\right] \tag{7}$$

where DBH is in meters. These mass components were then used to determine the crown density (ρ_{crown}) for each load case as follows:

$$\rho_{crown} = \begin{cases} M_B/V_{crown}, & \text{load case 1} \\ (M_B + M_F)/V_{crown}, & \text{load case2} \end{cases} \tag{8}$$

where V_{crown} is the total volume of the crown. This volume was estimated as a hemisphere of diameter d_{crown} as follows:

$$V_{crown} = \frac{2\pi}{3}\left[\frac{d_{crown}}{2}\right]^3 \tag{9}$$

The crown diameter (d_{crown}) is then given by the regression equation

$$d_{crown} = \frac{17.845 + 1.022 \times (\mathrm{DBH}/0.0254)}{3.281} \quad (\text{in meters}) \tag{10}$$

where DBH is in meters (Lamson, 1987). Similar to Equation 1, reliable species-specific allometric equations or parameters were not found in the literature; consequently, Equation 10 is used to estimate the crown diameter for each tree species in this study.

The leaf cluster approach developed by Honda and Fisher (1979) was used to distribute spherical clusters in the model, as an approximation for the observed leaf distribution in branches. The leaf cluster approach applied on a random tree is shown two-dimensionally in Figure 3. Spheres were placed at each splitting node beginning at the top of the trunk and ending at the third iteration nodes. Each sphere had a radius equal to 80% of the length of the longest distal element (Honda & Fisher, 1979). The 15 15 interaction volume matrix between the spheres was calculated analytically using a MATLAB function developed by Jacquenot (2022b). The intersection, or overlap, volume between the interacting spheres was distributed to each sphere in equal parts resulting in an adjusted volume (V_j) for the jth sphere (j ¼ 1; 2;...; 15) to satisfy the leaf cluster approach. This volume was multiplied by ρ_{crown} (Equation 8) to calculate the biomass distributed to the associated node for determining the loads to be applied.

Ice loads were calculated for two cases, one without the effects of leaves and one with the effects of leaves. The ice load case without leaves takes into consideration only the ice on the branches of the tree. Comparatively, the ice load case with leaves takes into consideration the ice on the branches and the ice on the effective leaf area. The mass of the ice on the branches and the leaves was calculated using their respective surface areas. The surface area for each element was calculated based on a cylinder, which was multiplied by the ice thickness (t_{ice}) to obtain the volume of ice for each element:

$$V_{ice,e} = t_{ice} \times 2\pi r_e l_e \tag{11}$$

where the element length (l_e) is determined by discretizing a branch into four equally spaced elements (see Figure 1). The ice's mass was then obtained by

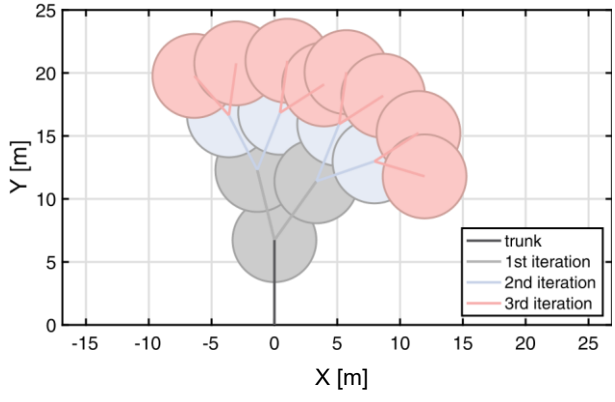

Figure 3. Leaf cluster approach with all three fractal iterations.

multiplying the volume of ice by the density of ice, ρ_{ice} ¼ 917 kg/m^3. The ice load for each element was then determined and distributed such that each end of the element received half of the element's ice load.

The ice mass on the leaves was calculated by using the effective leaf area where the effective leaf area was determined similar to the clustering approach outlined above, except with circular areas (Jacquenot, 2022a) instead of spherical volumes. It is important to note that the third iteration branches, biomass, and ice loads for loads cases 1 and 2 were included as point loads at the ends of their corresponding second iteration branches. The third iteration branch geometries and loads were calculated along with the first and second iteration fractals using the same method discussed in Section 2.1. Similarly, the biomass and ice loads due to the third iteration branches for both load cases 1 and 2 were determined using the methods outlined in this section.

Figure 1(b) shows the comparison between the two load cases – one without leaves and one with leaves – applied to a randomly generated tree. The increase in weights for the tree branches shown in Figure 1(b) due to an ice accumulation of 25.4 mm is 1.3 and 4.8 times for load cases 1 and 2, respectively. For load case 1, the average weight increase for all four tree species due to an ice accumulation of 25.4 mm was found to be about double that of the branches weight with an average standard deviation of 0.7 for the ice-branch weight multiplier. Comparatively, for load case 2, the average weight increase due to an ice accumulation of 25.4 mm was found to be nine times higher for Beech, Basswood, and Oak and 12 times higher for Sugar Maple with standard deviations of 16, 7.3, 5.3, and 7.5 for Sugar Maple, Beech, Basswood, and Oak, respectively. These values are comparable to the increases in branch weight due to ice accumulation reported by Hauer, Wang, and Dawson (1993).

2.4. Finite element method and analysis

The FE software OpenSees (McKenna & Feneves, 2000) was utilized to create and solve the FE model of the two-dimensional fractal tree. An example of a seven-element two-branch tree is shown in Figure 1(a). The tree was modeled with 29 nodes and 28 elements with each element being modeled as an Euler-Bernoulli beam element (*elasticBeamColumn*). A corotational geometric transformation, generally used with structures that experience large displacements and small strains, was used to transform the elements based on a local coordinate reference frame. A static analysis was performed using the Newton algorithm and 2% load increments. This analysis was performed for each of the 10,000 randomly generated trees for both load cases 1 and 2 for four tree species. The outputs that were recorded include the local element forces – axial forces (F_x) and bending moments (M_z) – and nodal displacements. The recorded local forces were used to compute the total stress for each element:

$$\sigma_{\max} = F_x/A_e \pm M_z/S_e \tag{12}$$

where $\sigma_{\max}$ is the maximum total stress, F_x is the axial force in the local x-axis, A_e is cross-sectional area of the element, M_z is the local bending moment at the ends of the element and S_e is the element's section modulus, which is equal to πr_e^4=4 for the circular cross-section.

2.5. Fragility curves

Fragility curves were developed for three branch damage states (DSs). These DSs were characterized by rupture due to the combined bending and axial stresses within a branch (Equation 12) exceeding MOR, i.e., failure occurring if $\sigma_{\max}$ MOR. In the fragility analysis, each tree was divided into two separate branch structures: left side (elements 5–16) and right side (elements 17–28) depicted in Figure 1(a). Consequently, the total number of analysed structures increased by a factor of two, resulting in N ¼ 20;000 branch structures per tree species for both load cases 1 and 2. For each branch structure, the first (ds_1), second (ds_2) and third (ds_3) damage states are characterized by at least one secondary branch failure, two secondary branch failures, and a primary branch failure, respectively. The fragility function is based on the probability of DS reaching or exceeding ds_i (i ¼ 1; 2; 3) given a specific intensity measure (t_{ice}):

$$\mathbb{P}[\mathrm{DS} \geq \mathrm{ds}_i \,|\, t_{\mathrm{ice}}] = \frac{1}{N}\sum_{i=1}^{N} \mathbb{I}_{\sigma_{\max}^{(i)} \geq \mathrm{MOR}} \tag{13}$$

where P½ is the probability, t_{ice} is the ice thickness, N is the total number of branch structures, and

$$\mathbb{I}_{\sigma_{\max} \geq \mathrm{MOR}} = \begin{cases} 1, & \sigma_{\max} \geq \mathrm{MOR} \\ 0, & \text{otherwise.} \end{cases} \tag{14}$$

When any branch failure occurs, the weight that is dropped (i.e., the fallen weight of a branch with ice) can be considered to be a fallen object that can potentially land on electrical components and disrupt or damage the electrical system. For this reason, the probability of having at least one secondary branch failure (DS ds_1) was used in the fallen weight (W) probability analysis.

The marginal probability of having a fallen weight of W given a certain ice thickness (t_{ice}) is expressed as

$$\mathbb{P}[W \mid t_{ice}] = \mathbb{P}[W, DS \geq ds_1 \mid t_{ice}] + \mathbb{P}[W, DS < ds_1 \mid t_{ice}] \quad (15a)$$

$$= \mathbb{P}[W \mid DS \geq ds_1, t_{ice}]\mathbb{P}[DS \geq ds_1 \mid t_{ice}] + \mathbb{P}[W \mid DS < ds_1, t_{ice}]\mathbb{P}[DS < ds_1 \mid t_{ice}] \quad (15b)$$

where the definition of conditional probability has been used to go from Equation 15a to Equation 15b, viz.

$$\mathbb{P}[W \mid D, t_{ice}] = \frac{\mathbb{P}[W, D \mid t_{ice}]}{\mathbb{P}[D \mid t_{ice}]} \quad (16)$$

for events D 2 fDS ds_1; DS < ds_1g. The probability shown in Equation 15b describes the potential scenarios for having fallen weight W. The first term of the first expression on the right-hand side of Equation 15b corresponds to the normalized PDF of W given that any branch failure occurred (DS ds_1) for a certain t_{ice}. The second term of the first expression on the right-hand side of Equation 15b corresponds to the fragility curve (Equation 13) where any branch failure occurred (DS ds_1) given a certain t_{ice}. The first term of the second expression on the right-hand side of Equation 15b corresponds to the case of having fallen weight W when no branch failures occurred (DS ds_1). This probability corresponds to the Dirac delta function, i.e., P½W jDS < ds_1; t_{ice} ¼ δðWÞ; hence, the results will be presented in terms of the cumulative distribution, which takes the form of a Heaviside function. The second term of the second expression on the right-hand side of Equation 15b corresponds to the complement of the Monte Carlo–based fragility curve where no branch failures occurred (DS < ds_1), i.e.,

P½DS < ds_1 jt_{ice} ¼ 1 P½DS ds_1 jt_{ice}. Also of interest is the expected fallen weight, which is given by

$$\mathbb{E}[W \mid t_{ice}] = \int_0^\infty w\mathbb{P}[w \mid t_{ice}]\,dw \equiv \mathbb{E}[W \mid DS \geq ds_1, t_{ice}]\mathbb{P}[DS \geq ds_1 \mid t_{ice}] \quad (17)$$

In the following section, results from the Monte Carlo sampling of tree responses are used to fit analytical expressions for the various probabilities discussed here.

3. Results and discussion

3.1. Tree deformation

A comparison of the displacements for each load case is shown in Figure 4 for a representative tree. Larger nodal displacements are developed in the load case with leaves (Figure 4(a)) than in the load case without leaves (Figure 4(b)). This is due to the leaves' surface area, which allows for more ice to accumulate (see Figure 1(b)) and leads to significantly larger displacements than the load case without leaves. Figure 4 shows that for both cases the secondary sections tend to have the largest nodal displacements for all ice thickness increments. Further, Figure 4(b) shows that tree branches that extend the furthest, perpendicular to the Y-axis, experience the largest deflections. This is due to the large moments produced by the increasing moment arm. It is interesting to note that in Figure 4, both load cases have a net deflection to the right of the initial position. This is counter-intuitive to the notion that the branches would deflect down and in the direction of the primary branch, orthogonal to the trunk. The direction of the deflection for each branch, and more importantly, the entire tree's final position, is influenced by the initial position of the tree and the interactions between the two branch structures (i.e., the left and right side of the tree). Further, this may be helpful to the electrical infrastructure when responding to a severe ice storm threat by pruning a portion of the tree that are near electrical components. This is because

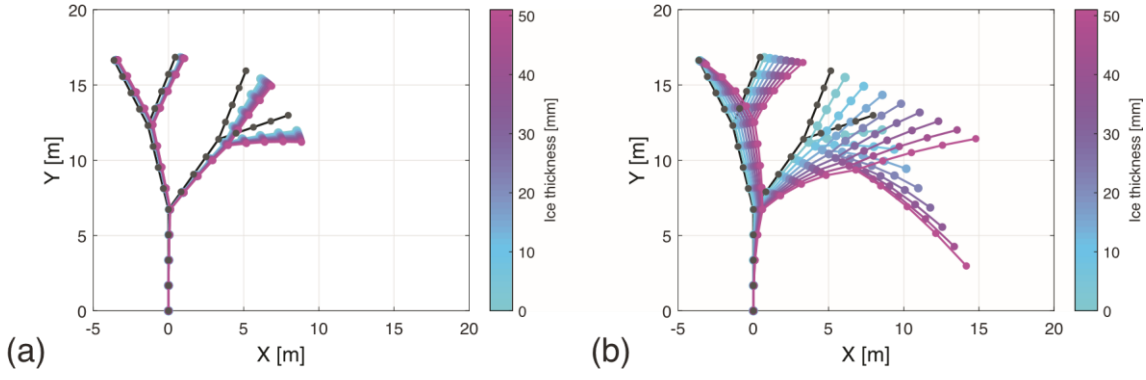

Figure 4. Comparison of nodal displacements between load case without leaves (left) and load case with leaves (right) at varying ice thicknesses.

pruning entire trees may be infeasible due to time constraints, especially if the trees are large. As shown in Figure 4(b), ice loads from the leaves produce large displacements and have the potential of causing a power outage from electrical arcing due to the tree branches completing the circuit between electrical lines. This is crucial in particular for electrical power distribution in urban areas, because shorts can occur even without the structural failure of a line or pole. Further, if the tree bears its weight on electrical components, the entire electrical line and the pole could fail structurally. Additionally, for a tree near a road, the displaced branches due to a severe ice storm, as shown in Figure 4(b), may cause a hazardous environment for traffic due to the obstruction caused by the deformed tree.

3.2. Fragility curves

Figure 5 shows the fragility curves (Equation 13) based on Monte Carlo sampling for the load cases without and with leaves for every damage state ds_i for the four tree species.

The Monte Carlo–based fragility curves shown in Figure 5 were fit assuming a log-normal cumulative distribution function (CDF):

$$F_{ds_i}(t_{ice}) = \mathbb{P}[DS \geq ds_i | t_{ice}] = \Phi\left(\frac{\ln(t_{ice}/\overline{t}_{ice,i})}{\beta_i}\right) \quad (18)$$

where ΦðÞ is the standard normal CDF, $t_{ice;i}$ is the median value of ice thickness t_{ice} at which the tree reaches the threshold of damage state (ds_i), and β_i is the logarithmic standard deviation for damage state ds_i. The fitted parameters and statistics for various damage states used in Equation 18 are shown in Table 2 for the cases without and with leaves. Table 2 shows a high coefficient of determination (R^2) for ds_1, ds_2, and ds_3 for both load cases. From Table 2, it is shown that there is not much variation between each predicted fragility curve's statistics within each species for the case without leaves. Comparatively, the case with leaves shows larger variations in the predicted fragility curve's statistics within each species. Figure 5 shows the fitted fragility curves predicted by Equation 18. It is observed that the predicted fragility curves trend well with the Monte Carlo–based fragility curves for both load cases without and with the effects of leaves.

For the case without leaves, the fragility curves for each ds_i are nearly identical for a given tree species, which indicates that tree branches under ice loads without leaves will likely fail in the primary section (ds_3). Additionally, because the failure occurs in the primary section, the secondary section branches will also fall with the primary section branch. The nearly identical

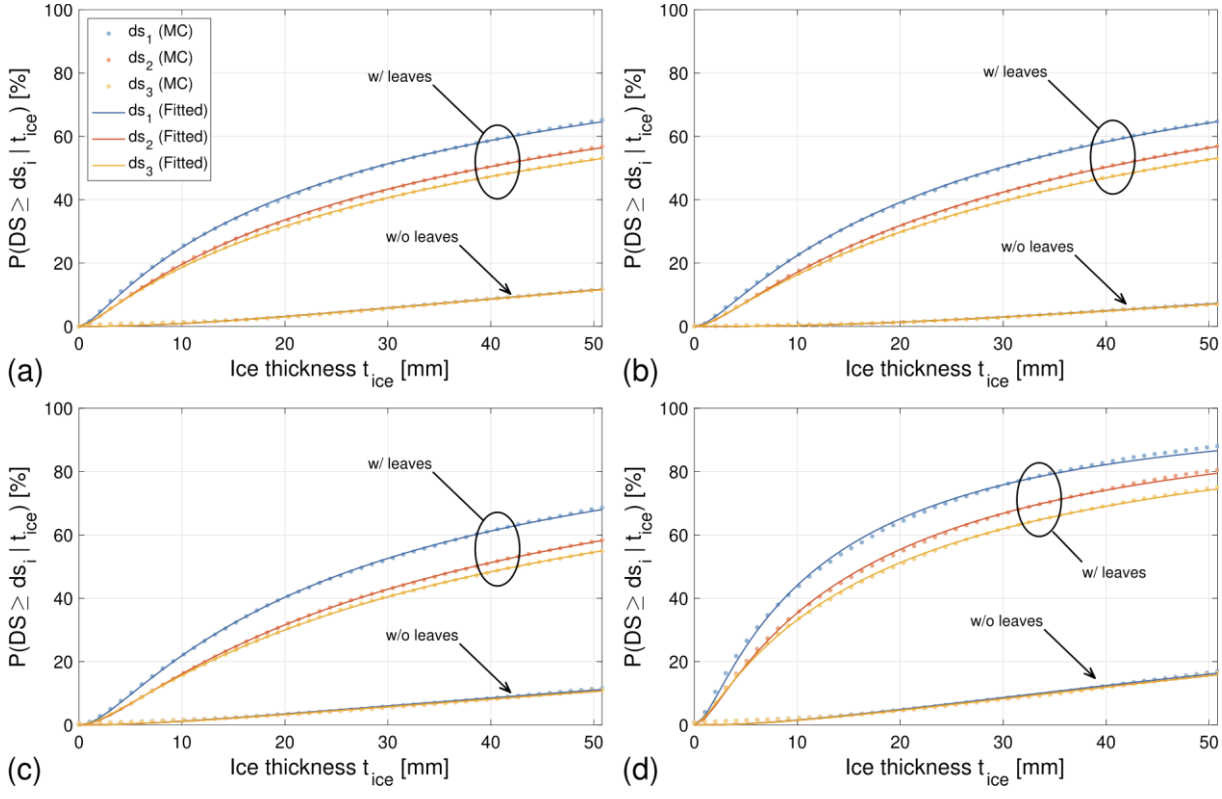

Figure 5. Fragility curves based on Monte Carlo (MC) simulation and fitted log-Normal distribution for all damage states ds_i without and with the effects of leaves for each tree species: (a) sugar maple, (b) beech, (c) basswood, and (d) white oak.

Table 2. Fitted parameters and coefficient of determination (R^2) for fragility curves (Equation 18).

			Tree Species			
Load Case	Damage State	Parameter	Sugar Maple	Beech	Basswood	White Oak
w/o leaves	ds_1	$t_{ice,1}$	265.6	308.9	339.7	196.6
		θ_1	1.392	1.238	1.561	1.380
		R_2	0.994	0.997	0.991	0.990
	ds_2	$t_{ice,2}$	264.5	314.5	352.8	201.5
		θ_2	1.383	1.242	1.562	1.375
		R_2	0.995	0.997	0.992	0.990
	ds_3	$t_{ice,3}$	264.8	314.5	353.2	202.4
		θ_3	1.383	1.242	1.563	1.378
		R_2	0.995	0.997	0.992	0.990
w/ leaves	ds_1	$t_{ice,1}$	28.47	29.64	27.55	12.11
		θ_1	1.546	1.431	1.307	1.294
		R_2	1.000	1.000	1.000	0.998
	ds_2	$t_{ice,2}$	39.25	39.61	38.32	16.63
		θ_2	1.596	1.447	1.358	1.357
		R_2	1.000	1.000	1.000	0.999
	ds_3	$t_{ice,3}$	44.75	45.11	42.48	19.09
		θ_3	1.682	1.531	1.436	1.486
		R_2	1.000	1.000	1.000	1.000

fragility curves for trees without leaves are potentially due to the trees' linearly decreasing geometric proportions and uniform ice distribution. It is also observed that the fragility curves for the case without leaves are low with failure probabilities of 11.7%, 7.2%, 11.6% and 16.9% at t_{ice} ¼ 50:8 mm for Sugar Maple, Beech, Basswood and White Oak, respectively.

For the cases with leaves, Figure 5 shows that there is a dramatic increase in the failure probability when compared to the case without leaves. For example, at t_{ice} ¼ 25:4 mm, the failure probabilities jumped by as little as 31% and as much as 65% due to the inclusion of leaves. Such increases in the probability of branch failure highlight the additional hazard posed by unseasonably early ice storms, like the October 2020 Oklahoma ice storm, when leaves are still on trees. Figure 5 additionally shows that fragility curves for the three damage states (ds_1, ds_2, and ds_3) differ from one another. This is because there are instances where one or two secondary branches fail, while the primary branch remains intact. This is due to the geometric shape of the trees and the distribution of leaves. Each tree has at least one branch that extends out away from the trunk, which develops larger bending stresses and increases the probability of failure compared to the branches closer to the trunk. Additionally, tree branches that are further from other tree branches also have a smaller interaction volume and area. These smaller

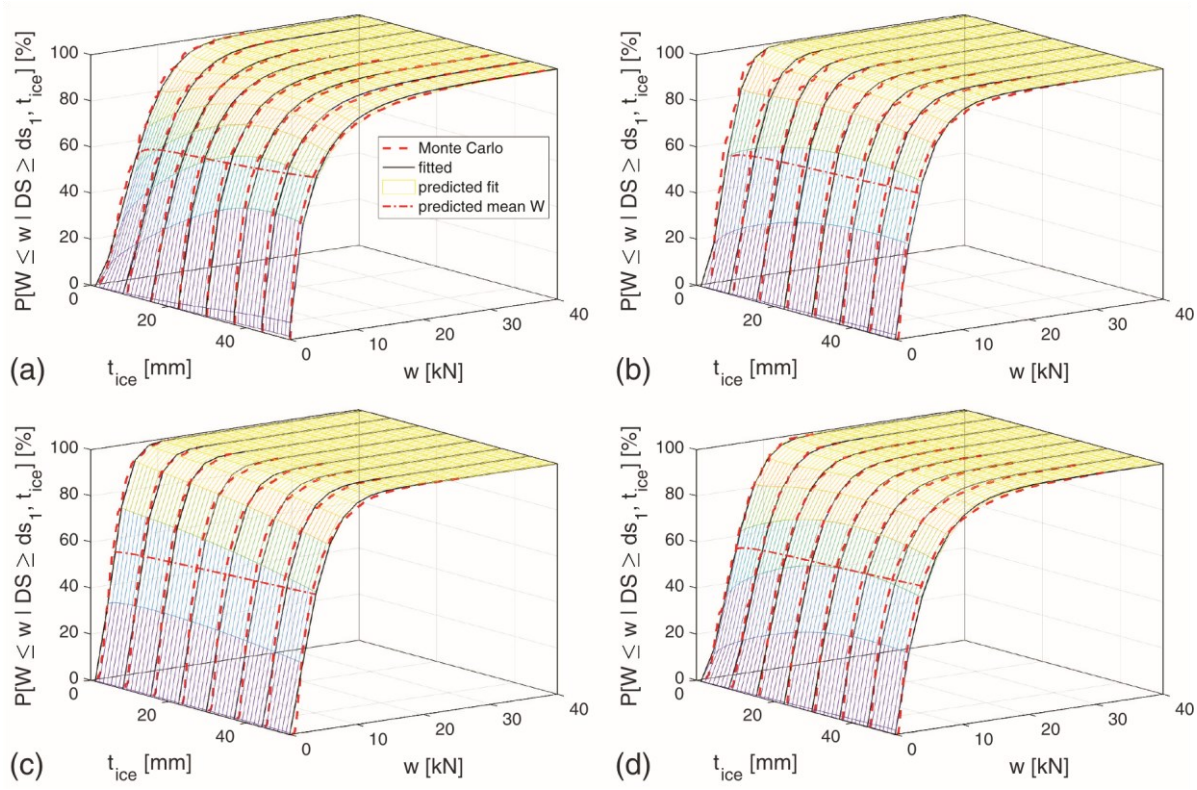

Figure 6. Cumulative probability of fallen weight W given that some damage is observed (DS $\geq$ ds_1) for a given ice thickness t_{ice} for each tree species—(a) sugar maple, (b) beech, (c) basswood, and (d) white oak—without the effects of leaves.

interactions result in branches that carry larger amounts of biomass and therefore carry more ice. The combination of large bending stresses and increased biomass and ice loads results in more instances of ds_1 or ds_2 occurring for every tree species. Consequently, White Oak (Figure 5(d)), a tree species with a relatively larger crown diameter, exhibits higher failure probabilities compared to the other tree species. For the cases with leaves, the differences between ds_1, ds_2 and ds_3 are similar for all four species, which indicates that each species experiences single and two branch failure instances similarly between species for the case with leaves. Leaves are shown to increase the likelihood of having a primary branch failure, which is important to mention due to the potential of having a large fallen weight. Further, the weight dropped from a primary section failure can be critical due to the possible addition of the weight of the secondary branches. Additionally, even though the weight dropped by a secondary branch failure is smaller than a primary branch failure, the increased probability of having a secondary failure is still important due to the potential of causing an electrical short when the fallen branch comes in contact with electrical lines. The variation in the fragility curves from one species to another is likely due to the geometric properties of each tree species (see Figure 2). It must be noted that a small portion of tree branches, for each species, failed under its own self- weight. These self-weight failures were small in quantity and were considered to be insignificant and therefore disregarded.

3.3. Fallen weight

Figures 6 and 7 show representative CDFs of fallen weight W based on Monte Carlo simulation, given that some damage is observed (DS $\geq$ ds_1) for the load cases without and with leaves, respectively, for the four tree species.

These distributions correspond to the first term of the first expression on the right-hand side of Equation 15b. A Weibull distribution was fitted to the Monte Carlo data for each tree species. At each ice thickness t_{ice}, the Weibull CDF is given by

$$F_W(w|\mathrm{DS} \geq \mathrm{ds}_1, t_{ice}) = \mathbb{P}[W \leq w|\mathrm{DS} \geq \mathrm{ds}_1, t_{ice}] = 1 - \exp\left\{-[w/A(t_{ice})]^{B(t_{ice})}\right\} \quad (19)$$

where $A(t_{ice})$ and $B(t_{ice})$ are the scale and shape parameters, respectively, which depend on the ice

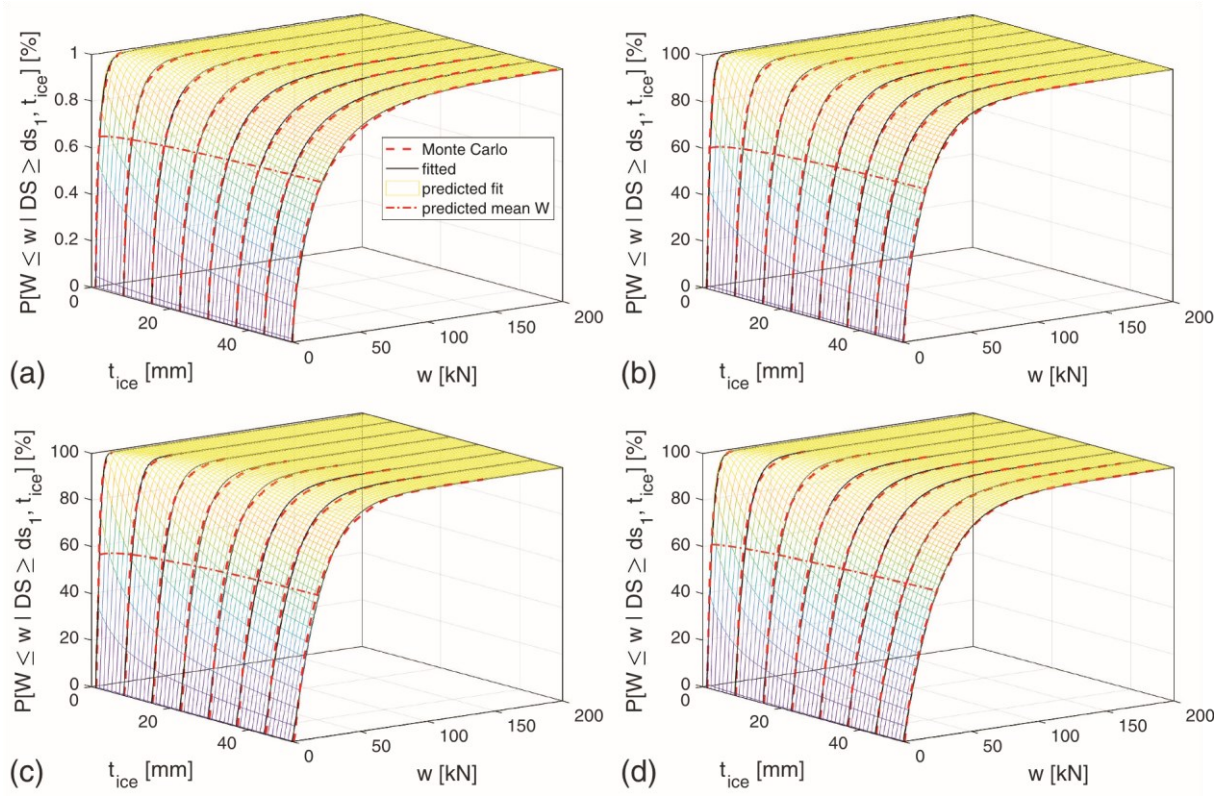

Figure 7. Cumulative probability of fallen weight *W* given that some damage is observed (DS ds$_1$) for a given ice thickness t_{ice} for each tree species—(a) sugar maple, (b) beech, (c) basswood, and (d) white oak—with the effects of leaves.

thickness. At each ice thickness, these parameters were fit to the Monte Carlo data, and the fitted parameters *A* and *B* are shown in Figures 8 and 9, respectively, for the trees without and with leaves at each ice thickness t_{ice}. Some representative fitted CDFs are shown in Figures 6 and 7.

The corresponding fitted Weibull parameters were then used to develop regression equations to predict the Weibull parameters with t_{ice}. The following regression equations are used for the Weibull scale parameter *A* and shape parameter *B*, respectively:

$$A(t_{ice}) = a_0 + a_1 t_{ice} + a_2 t_{ice}^2 \quad (20)$$

$$B(t_{ice}) = b_0 + b_1 t_{ice} + b_2 \ln(t_{ice}) \quad (21)$$

where a_0, a_1, a_2, b_0, b_1, and b_2 are the regression coefficients (hyperparameters). Figures 8 and 9 show the fitted curves for the Weibull parameters *A* and *B*, respectively, along with the fitted regression equations and coefficients of determination (R^2). It is observed from Figures 8 and 9 that the regression equations trend well with the fitted Weibull parameters. Further, Figures 8 and 9 show high R^2 values for the Weibull scale parameters *A* and *B* for the cases without and with leaves. The overall high R^2 values of the regression equations in Figures 8 and 9 show that the regression equations are suitable for predicting the Weibull parameters for a given ice thickness t_{ice}. The Weibull parameters predicted with Equation 20 and Equation 21 were then used to construct the predicted Weibull CDF surfaces (Equation 19) shown in Figures 6 and 7. It is observed from Figures 6 and 7 that the fitted and predicted CDFs trend well with the Monte Carlo CDF for all t_{ice} values and tree species. Importantly, these equations can be used to predict fallen weights for ice thicknesses other than those calculated based on the Monte Carlo analysis.

From Figures 6 and 7, there is an apparent difference in the distribution of *W* among the tree species given some level of damage (DS ds$_1$). For example, for the load case without leaves at t_{ice} ¼ 50:8 mm, the expected values (coefficients of variation) of *W* are 4.24 kN (1.41), 3.72 kN (0.949), 3.93 kN (0.748), and 4.53 kN (0.938) for Sugar Maple, Beech, Basswood, and White Oak, respectively. For the load case with leaves at t_{ice} ¼ 50:8 mm, the expected values (coefficients of variation) of *W* are 21.89 kN (1.26), 17.12 kN (1.07), 19.82 kN (0.868), and 24.54 kN (0.935) for Sugar Maple, Beech, Basswood, and White Oak, respectively. For both load cases, the Sugar Maple and White Oak have the higher expected *W*, with Sugar Maple having the highest

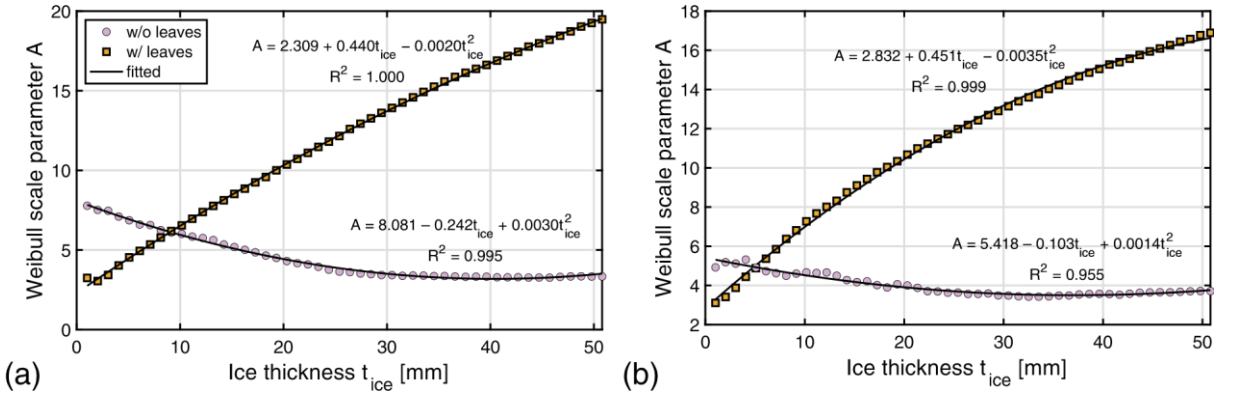

variation in both cases. Given some level of damage, the expected dropped weight *W* is around five times higher for the load case with ice than without ice.

From the foregoing discussion, not only are the probabilities of failure higher for the load case with leaves (see Figure 5) but the expected dropped weight *W* is also much higher (see Figures 6 and 7). Equation 15b captures this combined effect of the tree fragility and branch weight, which is shown in Figure 10 in the form of the CDF for the Sugar Maple without and with leaves. There is an instantaneous jump in the probability at $W = 0$ due to the probability of not having a failure, associated with the second expression on the right-hand side of Equation 15b. Then, for the cases with failures, there is a distribution of the weights expected to fall, associated with the first expression on the right-hand side of Equation 15b. Portrayed in this way, the effect of leaves is more pronounced, i.e., higher failure probabilities and fallen weight given failure. Figure 11 shows the expected fallen weight with ice thickness (Equation 17) for all four species without and with ice. The expected fallen weights for trees with leaves are about 30 to 40 times higher than for trees without leaves, exhibiting the compounding effect of higher probabilities of failure (fragility) and greater expected weight drop given a failure. Even though the Sugar Maple and White Oak showed similar expected dropped weights given a branch failure (DS ds_1), the expected fallen weight – considering cases with and without failures – for the White Oak is significantly higher because it was the more fragile tree (see Figure 5).

3.4. Implications for ice-storm resilience assessments

The fragility curves and fallen weight distributions developed in this study have implications for future resilience assessments considering ice storms (Hou, Muraleetharan, Panchalogaranjan, et al., 2023). In particular, hazards from fallen branches could be integrated into models of electrical and transportation networks. Given a geo-spatial distribution of ice accretions, fallen weight from trees in proximity to

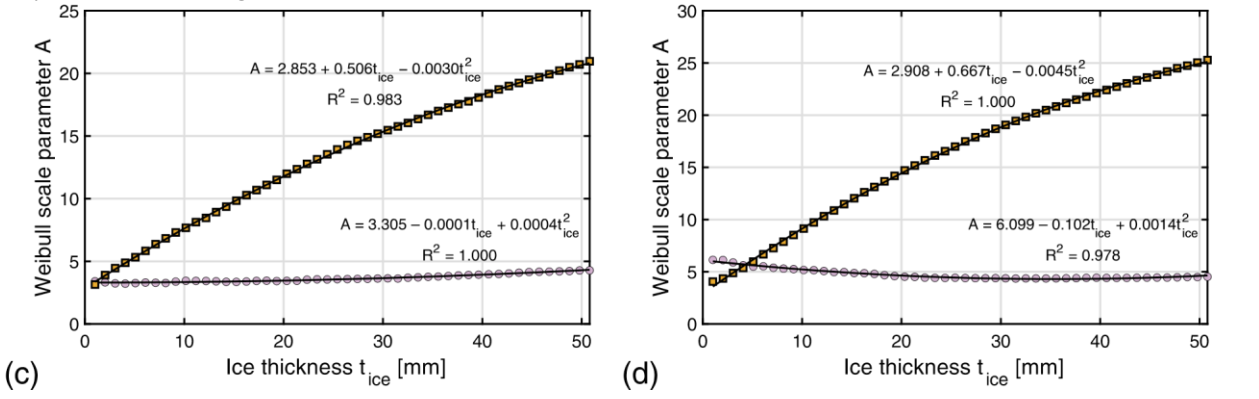

Figure 8. Variation of Weibull scale parameter *A* with ice thickness t_{ice} for each tree species—(a) sugar maple, (b) beech, (c) basswood, and (d) white oak—without and with the effects of leaves.

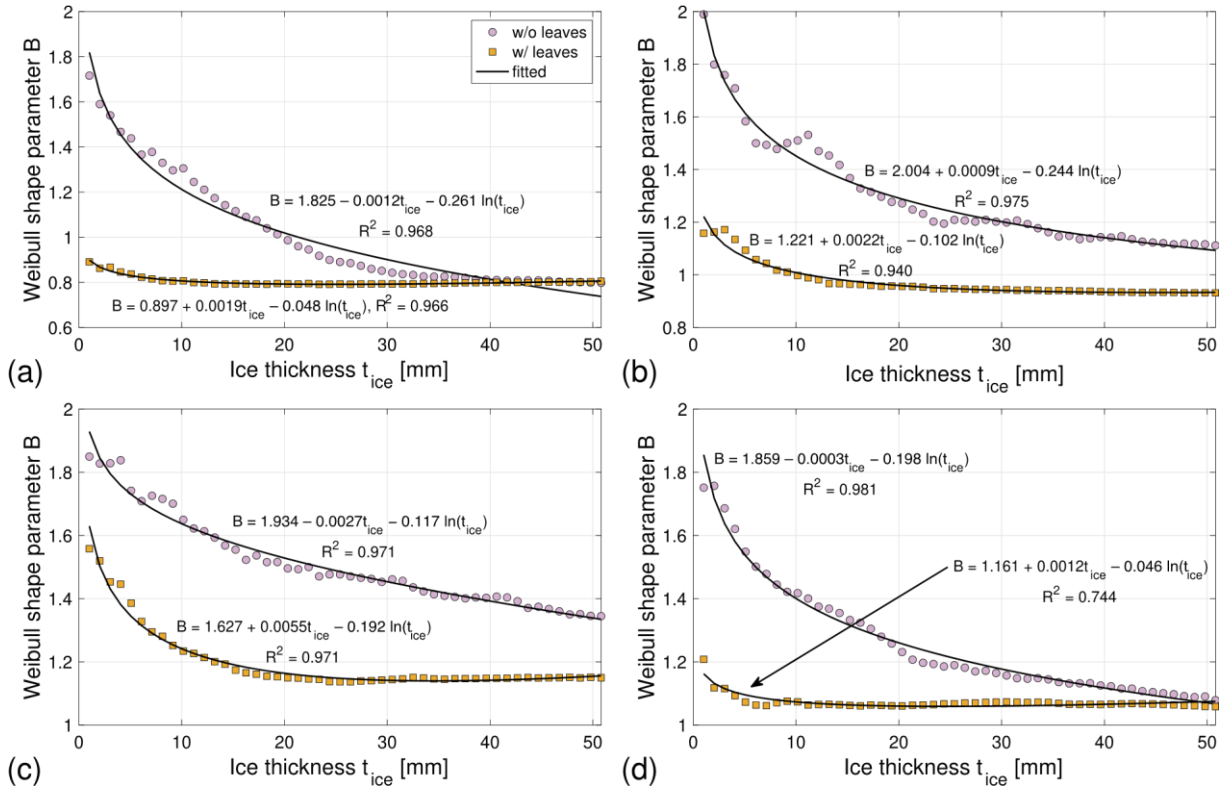

Figure 9. Variation of Weibull shape parameter B with ice thickness t_{ice} for each tree species—(a) sugar maple, (b) beech, (c) basswood, and (d) white oak—without and with the effects of leaves.

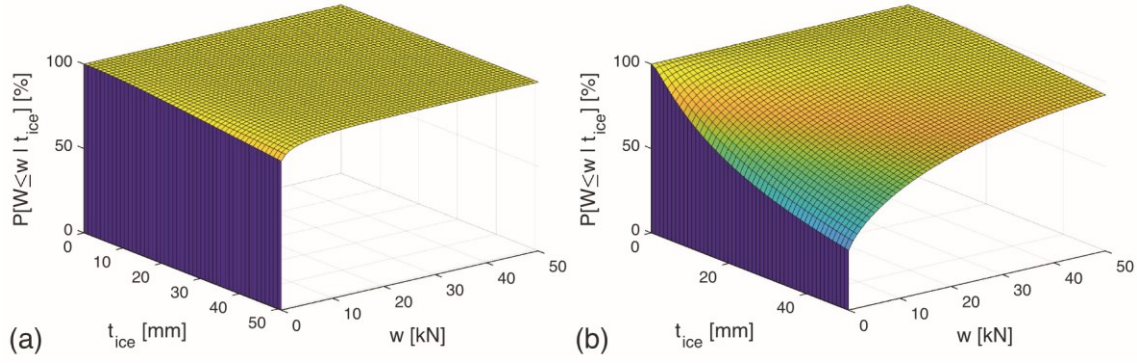

Figure 10. Cumulative probability of fallen weight W for a given ice thickness t_{ice} for the sugar maple without (a) and with (b) the effects of leaves.

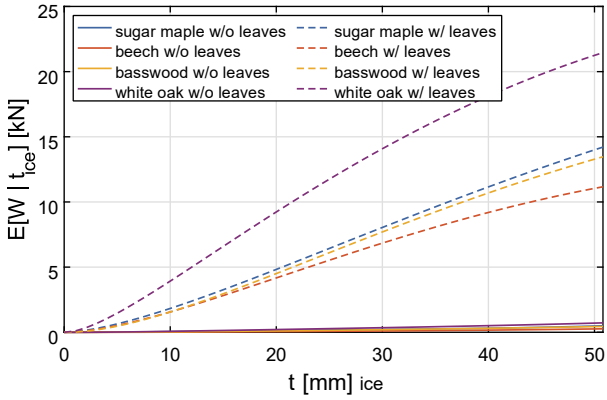

Figure 11. Variation of the expected fallen weight W with ice thickness t_{ice} for each tree species without (—) and with (– – –) the effects of leaves.

roads or power lines could be predicted. In a resilience framework using Monte Carlo sampling, this would involve randomly generating fallen weights from the distribution in Equation 15b. This would involve first generating a uniform random variable U,U½0; 1, which would be compared to the probability of failure determined from the fitted fragility curve, i.e., Equation 18 with parameters $t_{ice;1}$ and β_1 taken from Table 2. If $U > F_{ds1}(t_{ice})$, the branch would not have failed, and W ¼

0; if $U > F_{ds1}(t_{ice})$, the branch would have failed, and a random fallen weight would be generated from a Weibull distribution with scale parameter $A(t_{ice})$ and shape parameter $B(t_{ice})$ determined from the regression Equation 20 and Equation 21, respectively. These randomly generated fallen weights would serve as loads on electrical lines or the like. It is important to note that the fragility curves presented herein need to be validated due to assumptions made in the tree parameters, development of the tree model, estimation of the leaf's surface area, and the assumption to treat ice accretion as linear (i.e., uniform ice thickness around elements).

4. Conclusions

Recent ice storms have demonstrated that trees have the potential to cause electrical outages, damage electrical poles, and create hazardous environments for vehicle drivers. In this study, fragility curves based on the Monte Carlo method were developed with fractal trees for a range of ice accumulation. Two scenarios were considered, one which includes the effects of leaves and one which does not include the effects of leaves. A method for generating the distribution of fallen weight W was also provided. The fragility curves show that the presence of leaves produces a significant increase in the probability of tree failure than in the case without leaves, which is important because of the occurrence of unseasonably early ice storms due to climate change. Branches with leaves experience large deformations due to the weight of ice, which may be hazardous due to the branch's potential interaction with roads, traffic, and nearby electrical components. When exposed to various amounts of ice accretion, the most vulnerable branches of the tree are those branches, which are furthest from the trunk. The developed fragility curves and fallen weight distributions will be useful for assessing resilience strategies and frameworks for future ice storms. Future research should consider a three-dimensional tree to better model the displacement of branches. Furthermore, more accurate allometric equations for determining the weight of leaves should be considered. Future research must consider more fractal iterations to better capture the weight of all branches. Wind loads should also be considered as they may increase the deformation of the entire tree resulting in new failure modes.

Acknowledgments

The authors thank Dr. Rodney Will for his expertise and assistance with regard to tree anatomy.

Disclosure statement

No potential conflict of interest was reported by the author(s).

Funding

This material is based upon work supported by the National Science Foundation under Grant No. 1946093 Any opinions, findings, and conclusions or recommendations expressed in this material are those of the authors and do not necessarily reflect the views of the National Science Foundation.

Notes on contributors

Mr. Richard Campos is a PhD Candidate in the School of Civil Engineering & Environmental Science at the University of Oklahoma. He is currently working with Oklahoma EPSCoR to provide resilience strategies for infrastructure systems by analyzing hazards (e.g., ice storms, wildfires, earthquakes, and winds), risk, and fragility of electrical and transportation infrastructure components to increase infrastructure resiliency in Oklahoma.

Prof. P. Scott Harvey Jr is an Associate Professor in the School of Civil Engineering & Environmental Science at the University of Oklahoma. His research is related to natural hazards, their effects on infrastructure, and techniques to mitigate their effects.

Dr. Guangyang Hou is a Postdoctoral Research Associate at the University of Oklahoma. His current research interests include infrastructure resilience, probabilistic risk analysis, traffic safety, and seismic and wind performance of bridges. He received his PhD degree from Colorado State University in 2019. He serves as a guest editor for a special issue in the journal Sustainability titled Towards Resilient Infrastructure".

ORCID

R. Campos http://orcid.org/0000-0002-9277-6281
P. S. Harvey Jr http://orcid.org/0000-0002-0565-3102

Data availability statement

Data will be made available on reasonable request.

References

Aktan, A. E., Brownjohn, J. M. W., Moon, F. L., Sjoblom, K. J., Bartoli, I., & Karaman, S. G. (2022). Civil engineer for urban livability, sustainability and resilience. *Sustainable and Resilient Infrastructure*, *7*(5), 480–491. https://doi.org/

10.1080/23789689.2021.1937776

Ansari, A., Rao, K. S., & Jain, A. K. (2022). Seismic vulnerability of tunnels in Jammu and Kashmir for post seismic functionality. *Geotechnical and Geological Engineering*, *41* (2), 1371–1396. https://doi.org/10.1007/s10706-022-02341- 0

ASCE. (2017). *Minimum design loads and associated criteria for buildings and other structures* (7-16 ed.). American Society of Civil Engineers (ASCE).

Brommit, A. G., Charbonneau, N., Contreras, T. A., & Fahrig, L. (2004). Crown loss and subsequent branch sprouting of forest trees in response to a major ice storm. *Journal of the Torrey Botanical Society*, *131*(2), 169–176. https://doi.org/10.2307/4126918

Call, D. A. (2010). Changes in ice storm impacts over time: 1886-2000. *Weather, Climate, and Society*, *2*(1), 23–35. https://doi.org/10.1175/2009WCAS1013.1

Ciftci, C., Arwade, S. R., Kane, B., & Brena, S. F. (2014). Analysis of the probability of failure for open-grown trees during wind storms. *Probabilistic Engineering Mechanics*, *37*, 41–50. https://doi.org/10.1016/j.probengmech.2014.04.002

Degelia, S. K., Christian, J. I., Basara, J. B., Mitchell, T. J., Gardner, D. F., Jackson, S. E., Ragland, J. C., & Mahan, H. R. (2016). An overview of ice storms and their impact in the United States. *International Journal of Climatology*, *36*(8), 2811–2822. https://doi.org/10.1002/ joc.4525

Dmitry. (2021). Generation of 2D fractal trees. Mathworks. https://www.mathworks.com/matlabcentral/fileexchange/29536-generation-of-2d-fractal-trees

Dolce, C., Erdman, J. (2022). 10 of the worst ice storms in U.S. history. Retrieved 26, July, 2022. Weather Underground. https://www.wunderground.com/article/storms/winter/news/2022-02-03-united-states-worst-ice-storms

Erberik, M. A. (2014). Seismic fragility analysis. In M. Beer, I. A. Kougioumtzoglou, E. Patelli, & I.-S.-K. Au (Eds.), *Encyclopedia of Earthquake Engineering*. pp. 10. Springer.

FEMA. (2003). *Multi-hazard loss estimation method: Earthquake model: HAZUS MR4 technical manual*. Federal Emergency Management Agency.

FEMA. (2023). Declared Disasters. Retrieved March 1, 2023. Federal Emergency Management Agency. https://www.fema.gov/disaster/declarations

Forest Products Laboratory. (1999). Wood handbook: Wood as an engineering material. Technical report. https://doi.org/10.2737/fpl-gtr-113 .

Guidotti, R., Chmielewski, H., Unnikrishnan, V., Gardoni, P., McAllister, T., & van de Lindt, J. (2016). Modeling the resilience of critical infrastructure: The role of network dependencies. *Sustainable and Resilient Infrastructure*, *1* (3–4), 153–168. https://doi.org/10.1080/23789689.2016.1254999

Gulick, D. (2011). *Beauty of fractals six different views*. American Mathematical Society.

Harmon, S. M. (2012). *Recurrence Relations, Fractals, and Chaos: Implications for Analyzing Gene Structure*. Honors thesis, Colby College.

Hauer, R. J., Wang, W., & Dawson, J. O. (1993). Ice storm damage to urban trees. *Arboriculture & Urban Forestry*, *19* (4), 187–194. https://doi.org/10.48044/jauf.1993.031

Honda, H., & Fisher, J. B. (1979). Ratio of tree branch lengths: The equitable distribution of leaf clusters on branches. *Proceedings of the National Academy of Sciences*, *76*(8), 3875–3879. https://doi.org/10.1073/pnas.76.8.3875 .

Honda, H., & Hatta, H. (2004). Branching models consisting of two principles: Phyllotaxis and effect of gravity. *FORMA*, *19*(3), 183–196.

Honda, H., Tomlinson, P. B., & Fisher, J. B. (1981). Computer Simulation of branch interaction and regulation by unequal flow rates in Botanical Trees. *American Journal of Botany*, *68*(4), 569–585. https://doi.org/10.1002/j.1537-2197.1981.tb07801.x

Honda, H., Tomlinson, P. B., & Fisher, J. B. (1982). Two geometrical models of branching of Botanical Trees. *Annals of Botany*, *49*(1), 1–11. https://doi.org/10.1093/oxfordjournals.aob.a086218

Hou, G., & Chen, S. (2020). Probabilistic modeling of disrupted infrastructures due to fallen trees subjected to extreme winds in urban community. *Natural Hazards*, *102*(3), 1323–1350. https://doi.org/10.1007/s11069-020- 03969-y

Hou, G., Muraleetharan, K. K., Panchalogaranjan, V., Moses, P., Javid, A., Al Dakheeli, H., Bulut, R., Campos, R., Harvey, P. S., Miller, G., Boldes, K., & Narayanan, M. (2023). Resilience assessment and enhancement evaluation of power distribution systems subjected to ice storms. *Reliability Engineering & System Safety*, *230*, [108964]. https://doi.org/10.1016/j.ress.2022.108964

Ismay, J. (2020). Oklahoma ice storms leave thousands without power on eve of early voting. Retrieved 2, March, 2023. New York Times. https://www.nytimes.com/2020/10/28/us/ice-storm-oklahoma.html

Jacquenot, G. (2022a). *Analytical intersection area between two circles*. Mathworks. https://www.mathworks.com/matlabcentral/fileexchange/15899-analytical-intersection-area-between-two-circles?s_tid=srchtitle

Jacquenot, G. (2022b). *Analytical intersection volume between two spheres*. Mathworks. https://www.mathworks.com/matlabcentral/fileexchange/18532-analytical-intersection-volume-between-two-spheres?s_tid=srchtitle

Jenkins, J. C., Chojnacky, D. C., Heath, L. S., & Birdsey, R. A. (2003). National-scale biomass estimators for United States tree species. *Forest Science*, *49*(1), 12–35. https://www.fs.usda.gov/treesearch/pubs/6996

Jenkins, J. C., Chojnacky, D. C., Heath, L. S., & Birdsey, R. A. (2004). *Comprehensive database of diameter-based biomass regressions for North American tree species*. Technical Report NE-319, USDA Forest Service. https://doi.org/10. 2737/NE-GTR-319

Jinasena, K. D. S., & Sonnadara, D. U. J. (2013). Computer simulation of tree development with random variations and probabilistic growth of branches. *Journal of the National Science Foundation of Sri Lanka*, *41*(3), 229–235. https://doi.org/10.4038/jnsfsr.v41i3.6058

Kak, S. (2022). New classes of regular symmetric fractals. *Circuits, Systems, and Signal Processing*, *41*(7), 4149–4159. https://doi.org/10.1007/s00034-022-01966-z

Kakareko, G., Jung, S., & Ozguven, E. E. (2020). Estimation of tree failure consequences due to high winds using

convolutional neural networks. *International Journal of Remote Sensing*, *41*(23), 9039–9063. https://doi.org/10.1080/ 01431161.2020.1797219

Kenefic, L. S., & Nyland, R. D. (1999). Sugar maple height-diameter and age-diameter relationships in an uneven-aged Northern Hardwood Stand. *Northern Journal of Applied Forestry*, *16*(1), 43–47. https://doi.org/10.1093/njaf/16.1.43

Khan, T., & Conway, T. M. (2020). Vulnerability of common urban forest species to projected climate change and practitioners perceptions and responses. *Environmental Management*, *65*(4), 534–547. https://doi.org/10.1007/s00267-020-01270-z

Khiripet, N., Viruchpintu, R., Maneewattanapluk, J., Spangenberg, J., & Jungck, J. R. (2010). Morphospace: Measurement, modeling, mathematics, and meaning. *Mathematical Modelling of Natural Phenomena*, *6*(2), 54–81. https://doi.org/10.1051/mmnp/20116202 Kircher, C. A., Nassar, A. A., Kustu, O., & Holmes, W. T. (1997). Development of building damage functions for earthquake loss estimation. *Earthquake Spectra*, *13*(4), 663–682. https://doi.org/10.1193/1.1585974

Klima, K., & Morgan, M. G. (2015). Ice storm frequencies in a warmer climate. *Climatic Change*, *133*(2), 209–222. https://doi.org/10.1007/s10584-015-1460-9

Kovacik, C., & Kloesel, K. (2014). *Changes in ice storm frequency across the United States*, pp. 21. http://www.southernclimate.org/publications/Ice_Storm_Frequency.pdf .

Laefer, D. F., & Pradhan, A. R. (2006). Evacuation route selection based on tree-based hazards using light detection and ranging and GIS. *Journal of Transportation Engineering*, *132*(4), 312–320. https://doi.org/10.1061/ (ASCE)0733-947X(2006)132:4(312)

Lamson, N. I. (1987). D.b.h./crown diameter relationships in mixed Appalachian Hardwood Stands. Research Paper. Broomall, PA: U.S. Department of Agriculture, Forest Service, Northeastern Forest Experiment Station. https://doi.org/10.2737/NE-RP-610 .

Lindenmayer, A., & Prusinkiewicz, P. (1996). *The algorithmic beauty of plants*. Springer-Verlag.

Li, G., Zhang, P., Luh, P. B., Li, W., Bie, Z., Serna, C., & Zhao, Z. (2014). Risk analysis for distribution systems in the Northeast U.S. under wind storms. *IEEE Transactions on Power Systems*, *29*(2), 889–898. https://doi.org/10.1109/TPWRS.2013.2286171

Ma, S., Chen, B., & Wang, Z. (2018). Resilience enhancement strategy for distribution systems under extreme weather events. *IEEE Transactions on Smart Grid*, *9*(2), 1442–1451. https://doi.org/10.1109/TSG.2016.2591885

MathWorks. (2021). *MATLAB, version 9.11.0.1873467*. The MathWorks Inc.

McKenna, F., & Feneves, G. L. (2000). *Open System for Earthquake Engineering Simulation (OpenSees)* (2.5.0 ed.). Pacific Earthquake Engineering Research Center, University of California.

McPherson, E. G., & Peper, P. J. (2012). Urban tree growth modeling. *Journal of Arboriculture & Urban Forestry*, *38*(5), 175–183. https://doi.org/10.48044/jauf.2012.025

Mostafavi, A. (2018). A system-of-systems framework for exploratory analysis of climate change impacts on civil infrastructure resilience. *Sustainable and Resilient Infrastructure*, *3* (4), 175–192. https://doi.org/10.1080/23789689.2017.1416845

Napolitano, J. (2015). *The Cantor Set as a Fractal and its Artistic Applications*. Bachelor's thesis, Colorado College.

National Weather Service. (2000). December 25-26, 2000: Ice Storm Strikes the ArkLaTex. https://www.weather.gov/shv/event_2000-12-25_ice_storm .

National Weather Service. (2007). The December 8-11, 2007 ice storm in Oklahoma. https://www.weather.gov/oun/events-20071208 .

National Weather Services. (2020a). Early and Icy start to Winter (October 25-28, 2020). https://www.weather.gov/lub/events-2020-202001026-wintry .

National Weather Services. (2020b). The ice storm of October 26-29, 2020. https://www.weather.gov/oun/events-20201026 .

National Weather Service. (2021). Snow/Ice maps and impacts summary from February 2021 back to back to back winter storms. https://www.weather.gov/rlx/2021- February-Winter-Storms .

Owens, F. C., Verrill, S. P., Shmulsky, R., & Ross, R. J. (2019). Distributions of modulus of elasticity and modulus of rupture in four mill-run lumber populations. *Wood and Fiber Science*, *51*(2), 183–192. https://doi.org/10.22382/wfs-2019-019

Picard, N., Saint-André, L., & Henry, M. (2012). *Manual for building tree volume and biomass allometric equations*. Food and Agriculture Organization of the United Nations (FAO).

Pitilakis, K., Crowley, H., & Kaynia, A. M. (editors). (2014). *SYNER-G: Typology definition and fragility functions for physical elements at seismic risk*. Springer Netherlands.

Proulx, O. J., & Greene, D. F. (2001). The relationship between ice thickness and northern hardwood tree damage during ice storms. *Canadian Journal of Forest Research*, *31*(10), 1758–1767. https://doi.org/10.1139/x01-104

Rahman, M. T. (2010). *Integration of geospatial techniques in the assessment of vulnerability of trees to ice storms in Norman, Oklahoma*. PhD thesis, University of Oklahoma.

Saupe, D. (1988). Algorithms for random fractals. In H.-O. Peitgen, & D. Saupe (Eds.), *The Science of Fractal Images* (pp. 71–136). Springer.

Semonin, R. G. (1987). Severe weather climatology in the Midwest and arboriculture. *Arboriculture & Urban Forestry*, *4*(6), 128–136. https://doi.org/10.48044/jauf.1978.031

Sharma, N., Tabandeh, A., & Gardoni, P. (2018). Resilience analysis: A mathematical formulation to model resilience of engineering systems. *Sustainable and Resilient Infrastructure*, *3*(2), 49–67. https://doi.org/10.1080/23789689.2017.1345257

Swaminathan, R., Sridharan, M., & Hayhoe, K. (2018). A computational framework for modelling and analyzing ice storms. https://doi.org/10.48550/arXiv.1805.04907 .

Takahashi, K., Arii, K., & Lechowicz, M. J. (2007). Quantitative and qualitative effects of a severe ice storm on an old-growth beech–maple forest. *Canadian Journal of Forest Research*, *37* (3), 598–606. https://doi.org/10.1139/X06-266

Tari, A. N., Sepasian, M. S., & Kenari, M. T. (2021). Resilience assessment and improvement of distribution networks against extreme weather events. *International Journal of Electrical Power & Energy Systems*, *125*, [106414]. https://doi.org/10.1016/j.ijepes.2020.106414

Tropea, B., & Stewart, R. (2021). Assessing past and future hazardous freezing rain and wet snow events in Manitoba, Canada using a pseudo-global warming approach. *Atmospheric Research*, *259*, [105656]. https://doi.org/10.1016/j.atmosres.2021.105656

Wang, Z. H. I., Zhao, M. I. N. G., & Qi-Xing, Y. U. (2001). Modeling of branching structures of plants. *Journal of Theoretical Biology*, *209*(4), 383–394. https://doi.org/10.1006/jtbi.2001.2252

Zentner, I., Gündel, M., & Bonfils, N. (2017). Fragility analysis methods: Review of existing approaches and application. *Nuclear Engineering and Design*, *323*, 245–258. https://doi.org/10.1016/j.nucengdes.2016.12.021